ISSN 1063-7710, Acoustical Physics, 2019, Vol. 65, No. 2, pp. 141–150. © Pleiades Publishing, Ltd., 2019.
Original Russian Text © Yu.S. Andriyakhina, M.M. Karzova, P.V. Yuldashev, V.A. Khokhlova, 2019, published in Akusticheskii Zhurnal, 2019, Vol. 65, No. 2, pp. 147–157.

NONLINEAR ACOUSTICS

Accelerated Thermal Ablation of Biological Tissue Volumes using HIFU beams with Shock Fronts

Yu. S. Andriyakhina[a], * , M. M. Karzova[a], P. V. Yuldashev[a], and V. A. Khokhlova[a]

[a] *Moscow State University, Faculty of Physics, Moscow, 119991 Russia*

**e-mail: julia_andriakhina@mail.ru*

Received July 13, 2018

Abstract—The paper presents the results of a numerical experiment comparing the rates of volumetric thermal ablation of bovine liver tissue *ex vivo*, generated by a multielement ultrasound array Sonalleve V1 3.0T (Philips Healthcare) using various exposure protocols. Pulsed sonications with the same time-average, but different peak power and duty cycle were modeled. The treatment trajectory consisted of a discrete set of single foci located at the center and along two concentric circles. Beam focusing in tissue was modeled using the Westervelt equation, the temperature field was calculated using the bioheat equation, and the threshold of tissue damage was determined according to the thermal dose formulation. It is shown that pulsed shock-wave exposures can provide up to three times faster volumetric ablation of tissue as compared to continuous quasi-harmonic wave treatments.

Keywords: high-intensity focused ultrasound, ultrasound surgery, multielement array, nonlinear effects, shock front, thermal ablation, thermal dose, numerical simulation, Westervelt equation

DOI: 10.1134/S1063771019020015

1. INTRODUCTION

The last two decades have shown the rapid development of high-intensity focused ultrasound (HIFU) medical applications for noninvasive tumor destruction in various organs: the uterus, prostate, liver, kidneys, and thyroid [1–3]. HIFU surgery operates by focusing a powerful ultrasound beam through a coupling medium into the target region, irreversibly damaging tissue either by thermal necrosis due to local heating or by mechanical action [4, 5].

Thermal ablation exposure protocols, in which tissue is sonicated by harmonic waves, have been conventionally used in clinical practice. For these established protocols, certain limitations have been revealed such as, primarily, slow volumetric ablation rates and uncertainty of the resulted ablated volume [6, 7]. To mitigate these limitations, the use of nonlinear pulsed sonication protocols has been proposed, in which the time-averaged beam power remains constant, while an increase in peak power is compensated by the corresponding decrease in duty cycle [8–10]. At high operating peak power outputs, nonlinear propagation effects lead to formation of high-amplitude shock fronts in the pressure waveform at the transducer focus. A sharp increase in ultrasound energy absorption at the shocks results in acceleration of thermal tissue ablation and generation of more localized lesions due to the weakening of thermal diffusion effects [10–13].

The feasibility of accelerated tissue heating using shock-wave exposures, as compared with the harmonic ones, has been studied in detail for single focus sonications. Super focusing of shock fronts combined with rapid heating by the shocks result in generation of single thermal lesions within milliseconds, with appreciably smaller dimensions comparing to those obtained using harmonic sonication [10–12]. With an increase in shock-wave exposure time, boiling is initiated in tissue in the focal region, which dramatically changes the shape and dimensions of the lesion [12]. Thus, the use of nonlinear effects to increase the efficacy of purely thermal ablation in a single focus without boiling is possible only to rapidly obtain very small lesions.

Clinical applications require ablation of large tissue volumes of at least a few cubic centimeters in a sufficiently small time frame. To achieve this, the transducer focus is moved along some trajectory—either continuously [14] or in discrete steps along a sequence of single foci [15, 16]. Multifocal configurations can be created using multielement phased arrays [17, 18]. However, due to thermal diffusion from the heated volume, side effects of tissue overheating in the near field of the beam may occur and challenges in treating tissues located near bones or vascular regions also arise [6, 19, 20]. The use of nonlinear exposures that rely on shock-wave heating at the transducer focus has a potential to mitigate these side effects; however, devel-

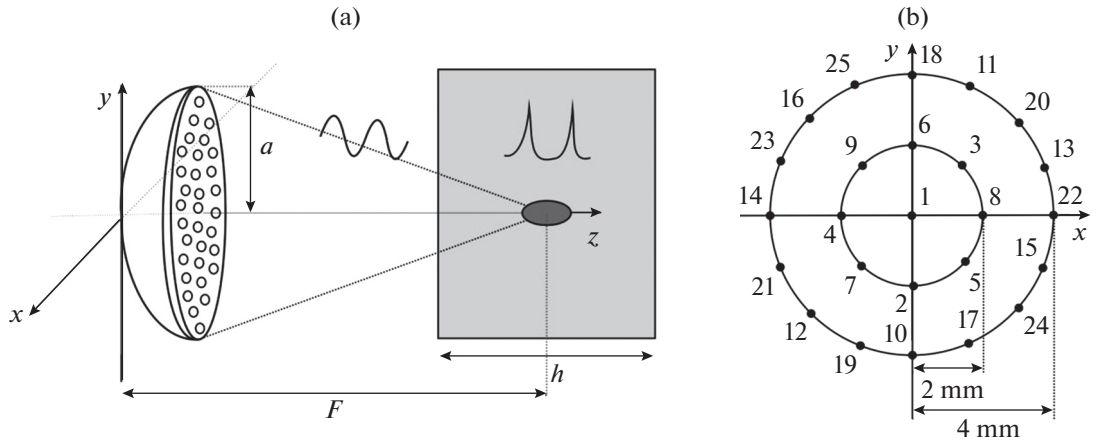

Fig. 1. (a) Scheme of the numerical experiment. Ultrasound beam is generated by a HIFU array with the aperture $2a = 128$ mm and focal length $F = 120$ mm; the array consists of 256 elements operating at a frequency of 1.2 MHz, a center of the curvature of the array surface is located at the center of liver tissue sample with thickness $h = 5$ cm; the transducer and the sample are placed in water. (b) Sequence of electronic movements of the array focus in the plane $z = F$ along a trajectory consisting of a discrete set of foci located on the two circles with radii of 2 and 4 mm. Points indicate centers of the generated single lesions.

opment of such exposures is still at the early stage of research [13, 16, 21].

The aim of this simulation study was to evaluate the efficacy of shock-wave exposure protocols that could be implemented for volumetric thermal tissue ablation in the existing clinical HIFU system.

2. FORMULATION OF THE PROBLEM

Figure 1 shows the geometry of the numerical experiment. The high-power phased array of the MRg HIFU Sonalleve V1 3.0T clinical system (Philips Healthcare) was considered as a HIFU transducer. The array consists of 256 round elements with a diameter of 6.6 mm and a frequency $f_0 = 1.2$ MHz arranged on a spherical segment with a radius $a = 64$ mm and focal length $F = 120$ mm [15, 22].

An ultrasound beam passed through a coupling medium (water) and focused at a depth of 2.5 cm in a $5 \times 5 \times 5$ cm bovine liver sample (Fig. 1a). The focus of the beam was translated perpendicular to the axis of the array. The initial sonication point was at the center of the sample and then the focus was moved along circular trajectories with radii of 2 and 4 mm, consisting of a discrete sequence of single foci with about 2 mm spacing (Fig. 1b). The sequence of the single foci on each circle was chosen so that the foci were at the maximum distance from each other (shown by numbers in Fig. 1b). Similar trajectory has been used in clinical practice; it has also been applied in recent experiments involving mechanical ablation of bovine liver tissue *ex vivo* using shock-wave exposure conditions [15, 16].

For comparison, two pulsed exposure protocols were chosen with intensities at the array elements of $I_{01} = 1.2$ W/cm^2 and $I_{02} = 15$ W/cm^2. The peak acoustic power of the array in the first protocol was 105 W, which is common for clinical use [7]. The second, high-output protocol with a peak power of 1.3 kW is achievable in this system when operating in research mode [16, 21, 22]. Earlier measurements and modeling of fields generated in this system when focusing in water demonstrated that the shock front starts to form at the focus at the transducer acoustic power of about 250 W [22]. Thus, in the first case of 105 W acoustic power, a quasi-linear focusing regime was realized. In the second case of 1.3 kW, high-amplitude shock fronts were present at the focus. The durations of tissue-heating pulses t_{heat} for single-focus sonication were chosen so that the total pulse energy was the same: $t_1 = 20$ ms for the quasi-harmonic regime and $t_2 = 1.6$ ms for the shock-wave regime. Single-focus steering along the trajectory was carried out simultaneously with the onset of each successive pulse, and the time interval between the movements was $\Delta t = 20$ ms.

3. NUMERICAL SIMULATION

3.1. Ultrasound Field and Heat Sources

Ultrasound beam propagation in water, and then in bovine liver sample, was modeled by the modified Westervelt equation, which takes into account nonlinear and diffraction effects, weak thermoviscous absorption, as well as the frequency–dependent absorption in tissue [10]:

$$\frac{\partial^2 p}{\partial\tau\partial z} = \frac{c_0}{2}\Delta p + \frac{\beta}{2\rho_0 c_0^3}\frac{\partial^2 p^2}{\partial\tau^2} + \frac{\delta}{2c_0^3}\frac{\partial^3 p}{\partial\tau^3} + L(p), \qquad (1)$$

where $p = p(x, y, z, \tau)$ is the ultrasound pressure; $\Delta = \frac{\partial^2}{\partial x^2} + \frac{\partial^2}{\partial y^2} + \frac{\partial^2}{\partial z^2}$ is the Laplace operator; z is the

coordinate along the beam axis; $\tau = t - z/c_0$ is the time in a retarted coordinate system; and parameters c_0, β, ρ_0, and δ are the sound speed, nonlinearity coefficient, ambient density, and diffusivity, respectively. Operator $L(p)$ is used to calculate absorption in the liver tissue, and it corresponds to the linear dependence of the absorption coefficient α_t on the frequency f and the logarithmic dispersion law that follows the causality principle [10, 11]:

$$\alpha_t(f) = \alpha_0 \frac{f}{f_0}, \quad \frac{c(f) - c_0}{c_0} = \frac{c_0\alpha_0}{\pi^2 f_0} \ln\left(\frac{f}{f_0}\right). \qquad (2)$$

Here α_0 is the absorption coefficient for tissue at a frequency f_0. The values of physical constants in Eq. (1) corresponded to a room temperature of 20°C and were $\rho_0 = 998$ kg/m^3, $c_0 = 1485$ m/s, $\beta = 3.5$, and $\delta = 4.33 \times 10^{-6}$ m/s for water, and $\rho_0 = 1050$ kg/m^3, $c_0 = 1580$ m/s, and $\beta = 4.0$ for bovine liver. The absorption coefficient α_0 for liver was assumed to be 8.43 m^{-1} at the frequency $f_0 = 1.2$ MHz [23].

Numerical solution to the Westervelt equation (1) was obtained using a previously developed algorithm described in detail in [10, 22, 24]. The boundary condition was first set at the spherical surface of the array as a uniform distribution of the particle velocity at the transducer elements and then was transferred to the plane passing through the apex of the transducer perpendicular to its axis [24]. The simulation results were used to determine the three-dimensional power density distribution of the heat sources $Q(x, y, z)$ in tissue, which was found as the loss rate for the total wave intensity when calculating the nonlinearity operator and absorption at each step of the spatial mesh dz along the beam axis [10, 24]:

$$Q(x, y, z) = -\frac{I(x, y, z + dz) - I(x, y, z)}{dz}, \qquad (3)$$

where $I(x, y, z) = I(\mathbf{r})$ is the sum of the intensities of all nonlinear wave harmonics:

$$I(\mathbf{r}) = \frac{1}{2\rho_0 c_0} \sum_{n=1}^{N} |p_n(\mathbf{r})|^2, \qquad (4)$$

$p_n(\mathbf{r})$ is the complex pressure amplitude of the nth harmonic of the wave in the Fourier expansion $p(\mathbf{r}, \tau) = \frac{1}{2} \sum_{n=-N}^{N} p_n(\mathbf{r}) \exp(-in\omega_0\tau)$. The number of harmonics N taken into account in simulating the Westervelt equation (1) varied from 1 to $N_{\max} = 800$ depending on the steepness of the pressure waveform in the solution. The heat sources $Q(\mathbf{r})$ were calculated at the nodes of the spatial mesh with the steps $dz = 0.1$ mm and $dx = dy = 0.025$ mm.

3.2. Temperature Field

The temperature field in the liver tissue sample was described by the heat transfer equation:

$$\frac{\partial T}{\partial t} = \chi \Delta T + \frac{Q}{C_v}, \qquad (5)$$

where $T(\mathbf{r}, t) = T(x, y, z, t)$ is the temperature in tissue, t is the time, χ is the thermal diffusivity coefficient, C_v is the volumetric heat capacity of the sample, and $Q(\mathbf{r})$ is the power density of the heat sources in tissue (3). The values of the physical parameters in Eq. (5) corresponded to bovine liver tissue and were $\chi = 1.93 \times 10^{-7}$ m^2/s, $C_v = 3.06 \times 10^6$ J/(m^3 °C) [10].

A direct approach for simulating Eq. (5) using finite-difference methods requires large datasets and time-intensive calculations because a change in temperature involves two strongly differing time scales: rapid local heating at a single focus and much slower heating of the total tissue volume under consideration. This paper proposes a method that takes into account such a difference in the time scales and results in substantial optimization of calculations. The simulation process was divided into two parts: auxiliary calculation of the temperature rise in a single heated focus in tissue and then simulation of heating the total tissue volume along the trajectory consisting of the single foci (Fig. 1b).

A spectral approach was used to simulate the temperature field in tissue. The solution $T(\mathbf{r}, t)$ of the heat transfer equation (5) was represented as a Fourier transform in the $\mathbf{k}$-space:

$$T(\mathbf{r}, t) = \int_{-\infty}^{\infty}\int_{-\infty}^{\infty}\int_{-\infty}^{\infty} \hat{T}(\mathbf{k}, t) \exp\left(2\pi i(k_x x + k_y y + k_z z)\right) \times dk_x dk_y dk_z, \qquad (6)$$

where the spatial spectrum components are

$$\hat{T}(\mathbf{k}, t) = \int_{-\infty}^{\infty}\int_{-\infty}^{\infty}\int_{-\infty}^{\infty} T(\mathbf{r}, t) \exp\left(-2\pi i(k_x x + k_y y + k_z z)\right) \times dx dy dz. \qquad (7)$$

After substitution of the expansion (6) into Eq. (5) and assuming that the heat sources $Q(\mathbf{r})$ are constant in time, the Eq. (5) transforms to the equation for the spatial spectral field components as follows:

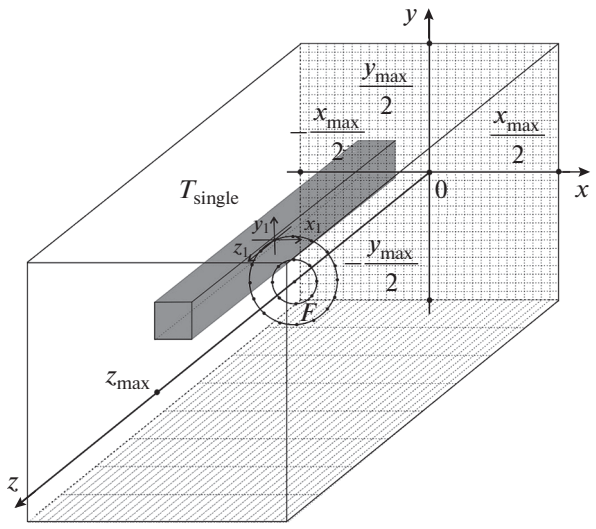

Fig. 2. Schematic representation of modeling the bioheat equation in a targeted volume in a spatial window with dimensions of $x_{max} \times y_{max} \times z_{max} = 30 \times 30 \times 40$ mm. Figure shows the geometry of calculation mesh: 1200 mesh nodes in the focal plane xy with spatial step of 0.025 mm and 400 nodes in axial direction of the beam z with step of 0.1 mm, as well as the trajectory of single foci in the plane $z = F$ of ultrasound beam. Volume of temperature distribution T_{single} of a single focus is shown in gray, which corresponds to linear sonication regime with initial intensity of 1.2 W/cm^2 at array elements.

$$\frac{\partial \hat{T}(\mathbf{k},t)}{\partial t} = -4\pi^2\mathbf{k}^2\chi\hat{T}(\mathbf{k},t) + \frac{\hat{Q}(\mathbf{k})}{C_v}, \tag{8}$$

for which an analytical solution exists:

$$\hat{T}(\mathbf{k},t) = \hat{T}_0(\mathbf{k})\exp\left(-4\pi^2\mathbf{k}^2\chi t\right) + \frac{\hat{Q}(\mathbf{k})}{4\pi^2\mathbf{k}^2\chi C_v}\left(1-\exp\left(-4\pi^2\mathbf{k}^2\chi t\right)\right). \tag{9}$$

Here $\hat{T}(\mathbf{k},t)$, $\hat{T}_0(\mathbf{k})$, $\hat{Q}(\mathbf{k})$ are the spatial Fourier spectra of the corresponding $T(\mathbf{r},t)$, $T_0(\mathbf{r})$, $Q(\mathbf{r})$ values and $T_0(\mathbf{r})$ is the initial temperature distribution in the volume under consideration. The spectra of the physical quantities $\hat{T}$, $\hat{T}_0, \hat{Q}$ were calculated in the Fortran environment using the fast Fourier transform (FFT) procedures included in the standard FFTW library.

First, heating at a single focus was calculated and solution was obtained for the temperature rise $T_{single}(\mathbf{r},\Delta t)$ in the vicinity of the focus during the time interval from $t = 0$ to $\Delta t = 20$ ms, which corresponded to the time when the transducer focus moved to the next point of the trajectory. Taking into account different sonication times for each of the two considered exposure protocols, the solution for the spatial spectrum of the temperature rise can be represented as a product of two time-dependent factors:

$$\hat{T}_{single}(\mathbf{k},\Delta t) = \frac{\hat{Q}(\mathbf{k})}{4\pi^2\mathbf{k}^2\chi C_v} \times \left(1-\exp\left(-4\pi^2\mathbf{k}^2\chi t_{heat}\right)\right) \times \exp\left(-4\pi^2\mathbf{k}^2\chi\left(\Delta t - t_{heat}\right)\right). \tag{10}$$

Here, the first factor describes the spatial spectrum of the temperature rise in a single focus at the end of the heating pulse with duration of t_{heat} (20 and 1.6 ms); the second one –at the moment Δt when the focus switched to the next point of the trajectory. It is assumed that the initial temperature distribution in the target focal region at $t = 0$ s was uniform, since each successive focal position was chosen at a sufficient distance from the preceding one (Fig. 1b).

The temperature distribution in the total tissue volume at each temporal step Δt of the mesh, from moment t to moment $t + \Delta t$, was calculated in three substeps. First, the solution to the diffusion equation (9) without heat sources was calculated in the k-space:

$$\hat{T}_{diff}(\mathbf{k},t+\Delta t) = \hat{T}(\mathbf{k},t)\exp\left(-4\pi^2\mathbf{k}^2\chi\Delta t\right). \tag{11}$$

Then, the solution (11) was converted to the spatial coordinates using (6) to determine $T_{diff}(\mathbf{r},t+\Delta t)$. At the third substep, the solution (10) that describes the result of a single exposure was transformed to spatial coordinates with the help of (6) and then superimposed on the resulting temperature distribution $T_{diff}(\mathbf{r},t+\Delta t)$:

$$T(\mathbf{r},t+\Delta t) = T_{diff}(\mathbf{r},t+\Delta t) + T_{single}(\mathbf{r},\Delta t). \tag{12}$$

This procedure (11–12) was performed successively at the moments when the focus was moved along the trajectory (Fig. 2).

Auxiliary calculation of a single exposure (6), (10) was carried out on a numerical mesh consisting of 480 nodes along each of the transverse coordinates x and y with a spatial step of 0.025 mm, and 400 nodes along beam axis z with a step of 0.1 mm (Fig. 2). The obtained distributions were truncated in each direction for each sonication protocol, so that the temperature increase at the boundary of the spatial window did not exceed 0.02°C. For initial intensity at the transducer elements of 1.2 W/cm^2, the window dimensions were 5.0 × 5.0 × 30 mm, and for the intensity of 15 W/cm^2, 2.5 × 2.5 × 14.0 mm.

When simulating volumetric tissue ablation, the size of the spatial steps were the same; the mesh consisted of 1200 nodes along each transverse coordinate x and y, and 400 nodes along the beam axis; i.e., the window dimensions were 30 × 30 × 40 mm (Fig. 2), and the time step corresponded to the movement time of the phased array focus $\Delta t = 20$ ms.

Such an approach makes it possible to calculate in advance the temperature distribution T_{single} for a single sonication, and then calculate the temperature field in the entire tissue sample with a large time step equal to the time between movements of the focus along the sonication trajectory.

3.3. Thermal Dose

The thermal dose value calculated at each point of the target area was used as the thermal ablation criterion [1, 10, 25]:

$$t_{56.0} = \int_0^{t_{\text{heat}}} R_0^{(56.0-T(\mathbf{r},t))} dt \geq 1.76, \qquad (13)$$

where $t_{56.0}$ is the time equivalent to the thermal dose measured with respect to the temperature of 56°C; R_0 is a coefficient taking a value of $R_0 = 0.5$ for $T(\mathbf{r},t) \geq 43$°C and $R_0 = 0.25$ for $T(\mathbf{r},t) < 43$°C. The thermal dose required to achieve the threshold for tissue ablation, $t_{56.0} = 1.76$ s, is commonly used in HIFU studies and corresponds to the dose determined for 43°C in hyperthermia: $t_{43.0} = 240$ min. In practice, thermal dose (13) is calculated from the MRI-measured temperature growth curve for the target region [7, 19, 26].

Since the thermal dose is an integral value, when modeling volumetric tissue ablation, the corresponding thermal dose distribution from a single sonication should be added to the thermal dose solution every $\Delta t = 20$ ms. Auxiliary calculation of the thermal dose for a single sonication was performed with respect to the initial temperature of 20°C with a time step of 16 μs during 20 ms. Then, when the dose distribution for a single sonication was added to the volumetric dose distribution, a correction to the initial temperature $T(\mathbf{r},t)$ at the corresponding focus was made:

$$t_{56.0} = \int_0^{t_{\text{heat}}} R_0^{56.0-[T(\mathbf{r},t)+\Delta T]} dt = D_0 R_0^{-\Delta T}, \qquad (14)$$

where $D_0(\mathbf{r},\Delta t)$ is a single dose calculated for an initial temperature of 20°C; ΔT is the difference between the temperature at the heating point and the initial temperature 20°C.

In simulations, the tissue was sonicated until the threshold value of the thermal dose was reached at the outer circle of 4 mm radius. Calculation of temperature and thermal dose was continued after HIFU was turned off until the moment when the growth of the ablated volume stopped due to the heat diffusion into surrounding tissue.

The distribution of a single thermal dose was first calculated in the same spatial window as the temperature for a single focus sonication; it was then truncated in all directions so that the value of the thermal dose did not exceed 0.01 at the boundary of the new window. For initial intensity of 1.2 W/cm^2 at the transducer elements, the window dimensions were 3 × 3 × 12 mm, and for initial intensity of 15 W/cm^2 – 1 × 1 × 6 mm.

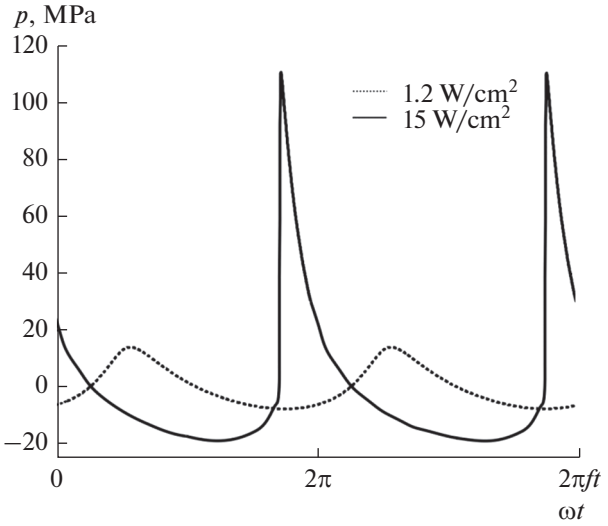

Fig. 3. Pressure waveforms at the focus for sonication of tissue sample with intensities of $I_0 = 1.2$ W/cm^2 (dotted line) and 15 W/cm^2 (solid line) at the array elements.

4. RESULTS AND DISCUSSION

4.1. Acoustic Field at a Single Focus

Figure 3 shows the pressure waveforms calculated at the focus of the HIFU transducer based on the Westervelt equation (1) for the two chosen sonication peak power outputs when focusing at a depth of 2.5 cm at the center of the liver tissue sample. The case with an initial intensity of $I_0 = 1.2$ W/cm^2 corresponds to quasi-linear focusing conditions, which is usually defined following the criterion that less than 10% of the full wave intensity is distributed over harmonics of the fundamental frequency [27–29]. For initial intensity of $I_0 = 15$ W/cm^2, high-amplitude shock fronts, at which effective absorption of ultrasound beam energy occurs, form at the focus in the wave profile. As is clear from the figure 3, the lower value of the shock is shifted to the domain of negative pressures. Such a wave profile corresponds to the onset of nonlinear saturation effects at the focus [28–31].

Figure 4 shows the power density distribution of heat sources Q in the liver sample obtained from numerical solution of the Westervelt equation. For initial intensity of 1.2 W/cm^2, when no shock fronts are present in the wave profile (Figs. 4a, 4b), the heat sources are distributed is much larger focal region than for initial intensity of 15 W/cm^2, when fully developed shocks had already formed at the focus (Figs. 4c, 4d)

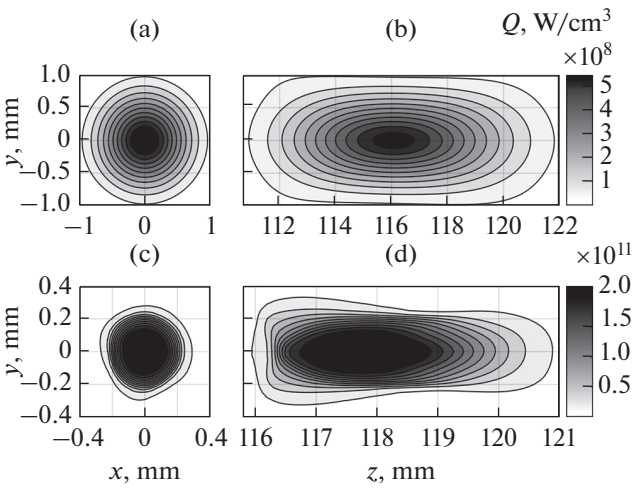

Fig. 4. Spatial power density distributions of heat sources in tissue in the (a, c) focal and (b, d) axial planes for (a, b) quasi-linear focusing conditions with initial intensity of $I_0 = 1.2$ W/cm^2 and (c, d) nonlinear shock-forming conditions with intensity of 15 W/cm^2 at the array elements.

[28, 29]. Due to sharp focusing of the shock fronts, the effective absorption of acoustic energy is concentrated in a small volume compared to the low-amplitude regime of focusing. Characteristic dimensions of the heating spot, determined by the level e^{-1} of the maximum, were 10 and 4 mm in the axial direction and 2 and 0.4 mm in the transverse direction in the focal plane for intensities of $I_0 = 1.2$ and 15 W/cm^2 at the transducer array elements, respectively. The corresponding intensities at the transducer focus were 3 and 47 kW/cm^2. For a 15.7-fold difference in intensities at the focus for the shock-wave regime in comparison to the quasi-harmonic one, there was a 411.3-fold difference in the maximum power density values of the heat sources. Thus, the regime with a fully developed shocks at the focus provided 26 times higher efficacy of the local heating of tissue.

Consider now in more detail the characteristics of tissue heating in a single focus for various intensities I_0 at the array elements within the operating range. Figure 5a shows the ratio of the power densities of the heat sources Q at the focus to the corresponding value in a linear beam Q_{lin} as a function of intensity I_0. At low intensities (up to 2 W/cm^2), Q/Q_{lin} is close to unity, then it increases dramatically within the range of intensities when shock fronts begin to form at the focus (4–5 W/cm^2). At the intensity level when fully developed shocks form at the transducer focus (vertical dotted line 2 in Fig. 5a), the density of heat deposition Q exceeds Q_{lin} in the linear beam by 35 times. With further increase in intensity, effects of nonlinear saturation of the shock amplitude in the focal waveform start to occur, which leads to a saturation in the dependence Q/Q_{lin} on the initial intensity [28–31]. In the saturation regime, the density of the heat deposition at the focal point becomes approximately 50 times larger than that in the linear beam (vertical dotted line 3 in Fig. 5a).

High spatial localization of the shock fronts within the focal region of the beam also leads to a significant (more than 20 times) decrease in the focal volume of the power density of heat sources in a nonlinear beam, determined, e.g., at a level of 10% of its maximum value (Fig. 5b). The minimum volume of the heat sources is reached in the case when the shock front just formed in the wave profile at the focus. With further increase in intensity at the transducer elements, the volume of the focal region slowly increased reaching twofold enlargement at the saturation level in comparison to the minimum volume. This effect is related to the formation of shock fronts in a larger region around the focus. Note that in the linear beam, the volume of the focal region of heat deposition does not change (dashed horizontal line in Fig. 5b).

Thus, in a nonlinear beam, the efficacy of heating at the focus sharply increases, but the dimensions of the focal region, in contrast, strongly decrease in comparison to the linear case. To simultaneously account for these two effects when evaluating the efficacy of heating finite tissue volumes in different focusing regimes, the total power of the heat sources W was calculated by integrating the power density Q over the volume of the focal region V_F: $W = \int_{V_F} Q dV$ (Fig. 4c). Calculations showed that the regime with fully developed shocks at the focus makes it possible to increase the heat deposition in the focal region up to twofold in comparison with the linear beam (vertical dotted line in Fig. 5c), and the maximum increase in the efficacy of heating in the saturation regime is up to 3.5 times.

To evaluate the efficacy of ultrasound tissue ablation, the change in the total acoustic beam power in the focal region and the distances at which the power losses are maximum were calculated. In the linear case, the total acoustic beam power in tissue decreases exponentially [1, 4]. The presence of shock fronts in the wave profile leads to additional generation of heat, the power of which is proportional to the shock amplitude cubed [4, 11, 12]. As shown in Fig. 6a, for nonlinear regimes with $I_0 = 6$–15 W/cm^2, the change in total beam power in the focal region appreciably deviates from the exponential law, in comparison to the quasi-linear regime ($I_0 = 1.2$ W/cm^2). Similarly, in strongly nonlinear regimes, when fully developed shocks have already formed at the focus, there is a sharp jump in heat release in a localized region near the focus $F =$ 120 cm (Fig. 6b). In the regime with the maximum shock amplitude, for $I_0 = 15$ W/cm^2, the layer of effective heat release is about 5 mm thick along the beam axis (vertical dashed lines in Fig. 6b). To generate volumetric ablation with dimensions exceeding 5 mm

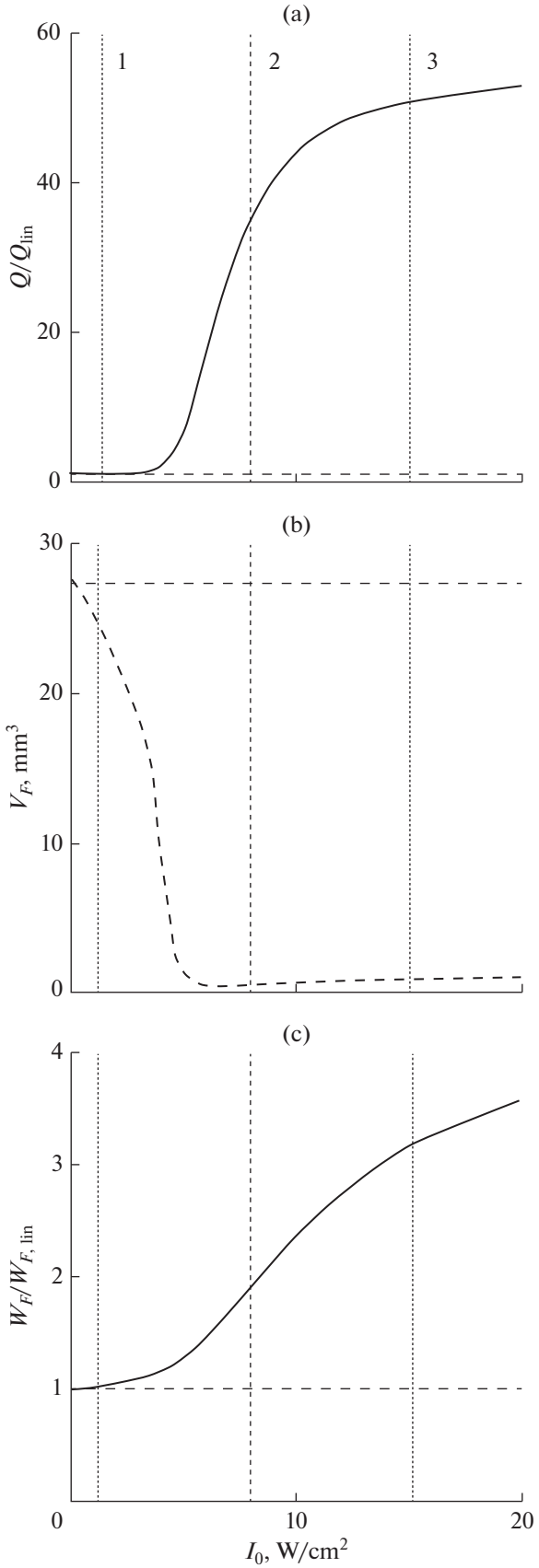

Fig. 5. Dependences of ultrasound heating parameters in tissue in the focal region of nonlinear beam generated by a multielement array with intensity I_0 at its elements (solid curves): (a) power density of heat sources Q at the focus, normalized to the corresponding value Q_{lin} in a linear beam; (b) volume of the focal region V_F of power density of heat sources, determined at the level of 10% of its maximum value; (c) power of heat sources W_F in the volume of the focal region $V_{F,lin}$, normalized to the corresponding value $W_{F,lin}$ in the linear beam. Dashed horizontal lines correspond to the case of linear focusing: $Q/Q_{lin} = 1$, $V_{F,lin} = 27.5$ mm^3, $W_F/W_{F,lin} = 1$. Vertical dotted lines 1, 2, and 3 correspond to the cases with initial intensity of 1.2 W/cm^2 (quasi-linear regime), 8 W/cm^2 (regime with fully developed shocks), and 15 W/cm^2 (saturation regime), respectively.

along the axial coordinate, it is possible to use layer-by-layer tissue ablation, for which sonication occurs at each layer along a trajectory of single foci and the distance between layers is on the order of 5 mm [16].

The importance of similar effects of sharp locally enhanced ultrasound absorption when shock fronts form near the focus has been noted in recent studies on the radiation force in the field of a focused Gaussian beam in absorbing medium [32]; on the mechanism of explosive instability of an overheated droplet in acoustic fountains using the model of standing wave evolution in a spherical resonator [33]; and on evaluating the possibility of employing HIFU to mechanically ablate brain tumors through an intact skull [34].

4.2. Temperature Field at a Single Focus

During a single sonication of 20 ms in the quasi-linear regime ($I_0 = 1.2$ W/cm^2), the tissue at the transducer focus was heated only by 3–4°C (Fig. 7a), while in the shock-wave regime ($I_0 = 15$ W/cm^2), the tissue reached boiling temperatures in about 1 ms (Fig. 7d). The growth in temperature at the focus during sonication in both cases was linear with time (Figs. 7a, 7d), which indicated the insignificant influence of diffusion effects during the given time intervals and, as a result, the predominant role of the second term in Eq. (9) over the first one. After the HIFU array was switched off, tissue temperature at the focus decreased due to the heat diffusion effect (Figs. 7a, 7d).

Comparison of the spatial temperature distributions in the focal plane (Figs. 7b, 7d) and along the beam axis (Figs. 7c, 7e) for the two sonication regimes with an initial intensity of 1.2 W/cm^2 (top row, Figs. 7b, 7c) and 15 W/cm^2 (bottom row, Figs. 7d, 7e) at the transducer elements identified the fundamental differences in the use of quasi-harmonic and shock-wave exposure protocols. First, the time required for thermal ablation of tissue differs by several orders of magnitude. For the low-intensity regime (Figs. 7b, 7c), by the time $t = 1.6$ ms, the spatial temperature distributions hardly changed at all with respect to the initial one, and the maximum growth at the center of the heating spot was only 0.3°C. For the shock-wave

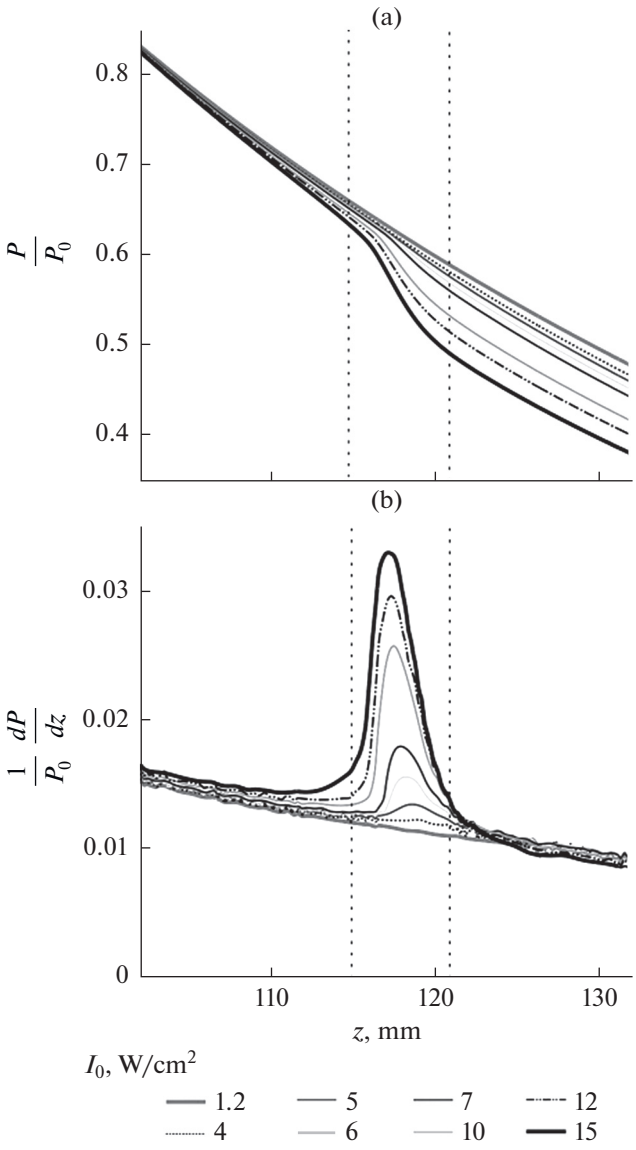

Fig. 6. Change (a) in total acoustic power P of the ultrasound beam and (b) losses of power dP/dz in tissue normalized to the initial acoustic power P_0 along the beam axis z for different intensity values I_0 at the array elements. Vertical dashed lines indicate the focal region of 5 mm length in which effective energy absorption is observed.

regime (Figs. 7e, 7f), within a sonication time $t = 1.6$ ms, the temperature at the center increased by 120°C and tissue ablation occurred in a 0.4 × 0.4 mm area in the focal plane and around 5 mm in the axial plane, which exactly corresponded to the dimensions of heat sources for the same initial intensity (Figs. 4c, 4d). Second, shock-wave regimes are promising in comparison to the quasi-linear regimes for suppressing diffusion effects, since tissue heating occurs very fast in a distinctly localized volume. Localization of thermal ablation is illustrated by the sharp temperature gradient along the z axis (Fig. 7e) in the focal region, and millisecond sonication proves sufficient for achieving boiling temperatures. In addition, cooling after the HIFU array is turned off also occurs quite quickly (Figs. 7e, 7f, case 100 ms).

Thus, when using shock-wave exposure protocols, the sharp decrease in the total acoustic beam power in the focal region and the rapid local heating of tissue at a single focus of the HIFU-array propose that it is possible to accelerate the thermal ablation process and obtain predictable ablation of clinically significant tissue volumes [11–13].

4.3. Ablation of a Clinically Significant Tissue Volume

Now consider parameters of the volumetric tissue ablation obtained in the case of the quasi-linear ($I_0 = 1.2$ W/cm^2) and nonlinear ($I_0 = 15$ W/cm^2) sonications along the circular trajectories (Fig. 1b). For the quasi-linear regime, sonication lasted 15.8 s, after which the thermal dose threshold was reached at the outer circle of the trajectory, and then cooling of tissue occurred in the course of 12 s. In the shock-wave regime, the sonication and cooling times were 4.6 and 7 s, respectively.

For the quasi-linear regime (Figs. 8a, 8b), uniform heating of tissue is obtained without sharp spatial temperature gradients within the ablated tissue volume (gray contour in Figs. 8a, 8b). For the nonlinear regime (Figs. 7c, 7d), the temperature distributions are less uniform, and within the contour delineating achievement of the thermal dose threshold, regions with temperature differing by more than 30°C are observed.

Thermal diffusion from the heated volume into the surrounding tissue layers in the axial direction is significantly stronger for the quasi-linear regime, than for the nonlinear one, resulting in an increase of the ablated region along the beam axis (Figs. 8b, 8d). In contrast, the ablated region in the nonlinear regime has distinct contours, which correspond to the initial contours of the heat sources (Figs. 4c, 4d). In such regime, the diffusion effects are strongly suppressed by rapid heating, which potentially reduces the risk of damaging surrounding tissues.

Clinical applications require achieving the ablation of tissue volumes with distinct boundaries within a sufficiently short time. The rate of developing such ablation was calculated as the ratio of the volume in which the thermal dose reached the threshold level to the sonication time. For the considered cases with initial intensities of 1.2 and 15 W/cm^2, the final ablated tissue volumes were 293 and 192 mm^3, respectively, while the rates of volumetric ablation were 18.5 and 41.7 mm^3/s. Thus, the gain in ablation rate when using the shock-wave regime ($I_0 = 15$ W/cm^2) was 2.3 times higher comparing to that for the quasi-linear regime ($I_0 = 1.2$ W/cm^2) conventionally used with the HIFU-array. More uniform heating of tissue in the shock-wave regime may be achieved by optimization of the sonication trajectory, i.e. by decreasing the distance between neighboring foci, as well as by controlling the

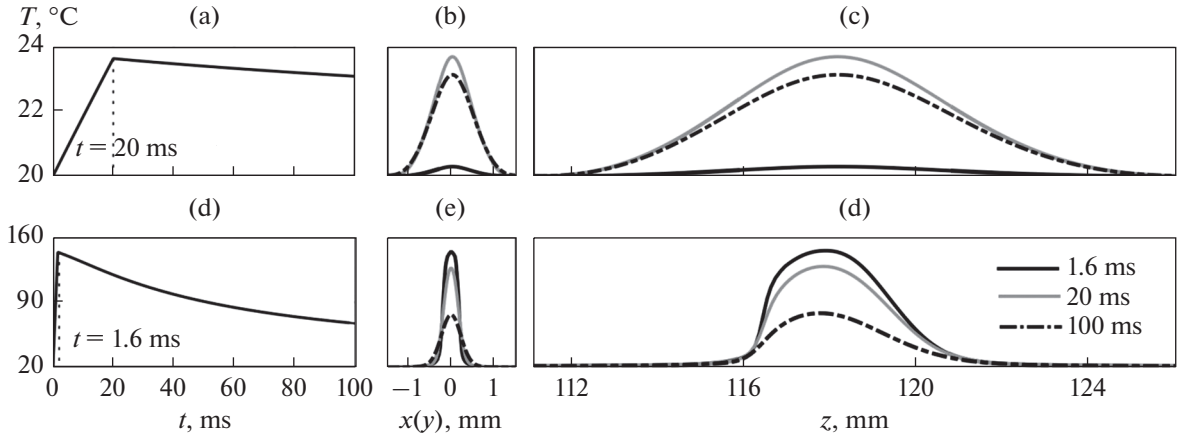

Fig. 7. Dependences of temperature at the array focus on time (a, g) and temperature distribution in the (b, e) focal and (c, f) axial planes of the ultrasound beam for quasi-linear (a–c, I_0 = 1.2 W/cm^2, sonication time, t = 20 ms) and shock-wave (d–f, I_0 = 15 W/cm^2, t =1.6 ms) sonication conditions at a single focus in tissue. Spatial temperature distributions (b, c, e, f) correspond to time instants of 1.6, 20, and 100 ms.

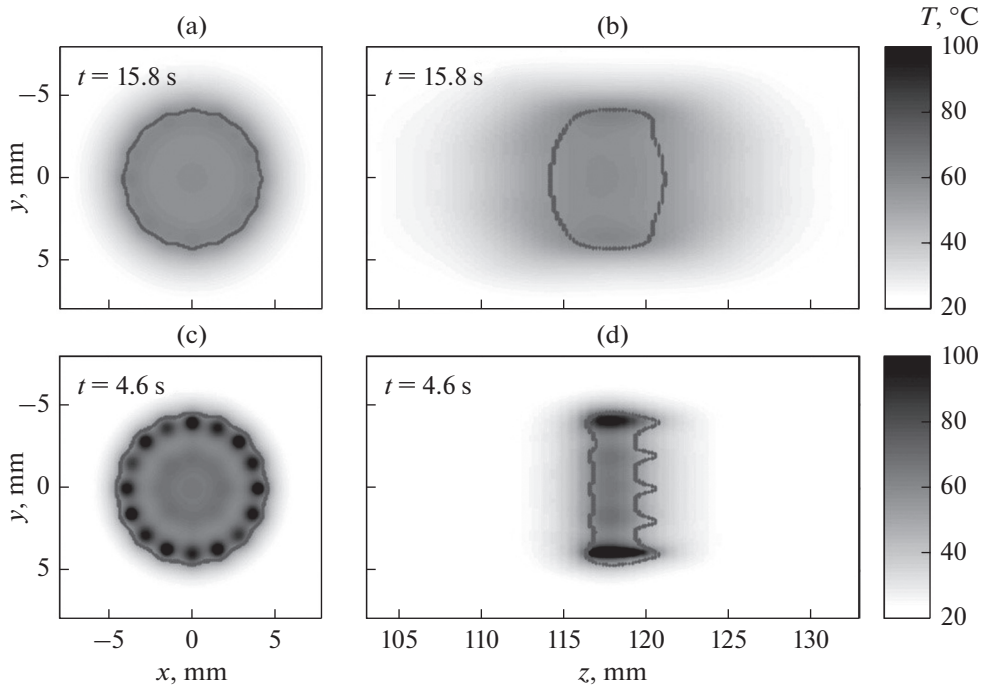

Fig. 8. Spatial temperature distributions at the end of volumetric tissue sonication in the (a, c) focal and (b, d) axial planes for intensities of (a, b) I_0 = 1.2 and (c, d) 15 W/cm^2 at the transducer elements. Sonication off time t is shown for each case. Gray contour shows the boundary of area within which thermal dose determined with respect to a temperature of 56°C reaches $t_{56.0}$ = 1.76 s after cooling of the sonicated tissue volume.

achievement of the thermal dose threshold at each of the trajectory circles .

5. CONCLUSIONS

An algorithm has been developed to simulate numerically volumetric thermal ablation of biological tissue, obtained using electronic steering the focus of the ultrasound phased array Sonalleve V1 3.0T (Philips Healthcare) along circular trajectories used in clinical practice. The efficacy of heating a clinically significant volume of biological tissue was compared for quasi-harmonic and shock-wave focusing regimes with the same time-averaged power, but different peak powers and duty cycles for pulsed sonication. It was shown that when the shock-wave sonication regime was used, tissue ablation rate increased approximately twofold in comparison to the quasi-harmonic regime,

and the obtained volumetric lesion corresponded in shape to the heated region due to suppression of heat diffusion along the beam axis. The results of numerical experiment also showed that to ensure more uniform heating of tissue with the shock-wave beam, an optimization of the sonication trajectory of single foci is required. The development of such trajectories, as well as protocols for treating several tissue layers to increase the final ablation volume, is a subject of further research toward improving medical HIFU technology.

ACKNOWLEDGMENTS

The study was supported by the Russian Science Foundation (grant no. 14-12-00974-P) and the Focused Ultrasound Surgery Foundation. The authors thank L.R. Gavrilov for helpful comments.

REFERENCES

1. *Physical Principles of Medical Ultrasonics,* Ed. by C. R. Hill, J. C. Bamber, and G. R. ter Haar, 2nd ed. (John Wiley and Sons, 2004; Fizmatlit, Moscow, 2008).
2. T. J. Dubinsky, C. Cuevas, M. K. Dighe, O. Kolokythas, and J. H. Hwang, Am. J. Roentgenol. **190**, 191 (2008).
3. L. R. Gavrilov, *High-Intensity Focused Ultrasound for Medicine* (Fazis, Moscow, 2013) [in Russian].
4. M. R. Bailey, V. A. Khokhlova, O. A. Sapozhnikov, S. G. Kargl, and L. A. Crum, Acoust. Phys. **49** (4), 369 (2003).
5. M. Hoogenboom, D. Eikelenboom, M. H. den Brok, A. Heerschap, J. J. Fütterer, and G. J. Adema, Ultrasound Med. Biol. **41** (6), 1500 (2015).
6. C. Mougenot, M. O. Köhler, J. Enholm, B. Quesson, and C. Moonen, Med. Phys. **38**, 272 (2011).
7. A. M. Venkatesan, A. Partanen, T. K. Pulanic, M. R. Dreher, J. Fischer, R. K. Zurawin, R. Muthupillai, S. Sokka, H. J. Nieminen, N. Sinaii, M. Merino, B. J. Wood, and P. Stratton, J. Vasc. Intervention. Radiol. **23** (6), 786 (2012).
8. V. A. Khokhlova, M. R. Bailey, J. A. Reed, B. W. Cunitz, P. J. Kaczkowski, and L. A. Crum, J. Acoust. Soc. Am. **119** (3), 1834 (2006).
9. K. Hynynen, Ultrasound Med. Biol. **36** (2), 85 (1987).
10. P. Yuldashev, S. Shmeleva, S. Ilyin, O. Sapozhnikov, L. Gavrilov, and V. Khokhlova, Phys. Med. Biol. **58** (8), 2537 (2013).
11. E. A. Filonenko and V. A. Khokhlova, Acoust. Phys. **47** (4), 468 (2001).
12. M. Canney, V. Khokhlova, O. Bessonova, M. Bailey, and L. Crum, Ultrasound Med. Biol. **36**, 250 (2010).
13. P. Ramaekers, M. De Greef, J. M. M. Van Breugel, C. T. W. Moonen, and M. Ries, Phys. Med. Biol. **61**, 1057 (2016).
14. F. Wu, Z. B. Wang, W. Z. Chen, W. Wang, Y. Gui, M. Zhang, G. Zheng, Y. Zhou, G. Xu, M. Li, C. Zhang, H. Ye, and R. Feng, Ultrason. Sonochem. **11**, 149 (2004).
15. M. O. Köhler, C. Mougenot, B. Quesson, and J. Enholm, Med. Phys. **36** (8), 3521 (2009).
16. V. A. Khokhlova, A. D. Maxwell, T. Khokhlova, W. Kreider, M. Bailey, A. Partanen, N. Farr, and O. Sapozhnikov, in *Proc. 14th Int. Symposium for Therapeutic Ultrasound* (Las Vegas, NV, 2014).
17. D. R. Daum and K. Hynynen, IEEE Trans. Ultrason., Ferroelectr. Freq. Control **45** (1), 208 (1998).
18. J. W. Hand, A. Shaw, N. Sadhoo, R. J. Dickinson, and L. R. Gavrilov, Phys. Med. Biol. **54** (19), 5675 (2009).
19. B. Quesson, M. Merle, M. O. Kohler, C. Mougenot, S. Roujol, B. D. de Senneville, and C. T. Moonen, Med. Phys. **37** (6), 2533 (2010).
20. J.-F. Aubry, M. Pernot, F. Marquet, M. Tanter, and M. Fink, Phys. Med. Biol. **53** (11), 2937 (2008).
21. A. Eranki, N. Farr, A. Partanen, K. V. Sharma, H. Chen, C. T. Rossi, S. V. Kothapalli, M. Oetgen, A. Kim, A. H. Negussie, D. Woods, B. J. Wood, P. C. W. Kim, and P. S. Yarmolenko, PLoS One **12** (3), e0173867-1-23 (2017).
22. W. Kreider, P. V. Yuldashev, O. A. Sapozhnikov, N. Farr, A. Partanen, M. R. Bailey, and V. A. Khokhlova, IEEE Trans. Ultrason., Ferroelectr. Freq. Control **60** (8), 1683 (2003).
23. F. A. Duck, *Physical Properties of Tissue* (Academic Press, London, 1990).
24. P. V. Yuldashev and V. A. Khokhlova, Acoust. Phys. **57** (3), 334 (2011).
25. S. A. Sapareto and W. C. Dewey, Int. J. Radiat. Oncol. Biol. Phys. **10** (6), 787 (1984).
26. D. Kopelman, Y. Inbar, A. Hanannel, D. Freundlich, D. Castel, A. Perel, A. Greenfeld, T. Salamon, M. Sareli, A. Valeanu, and M. Papa, Eur. J. Radiol. **59**, 157 (2006).
27. *IEC TS No. 61949: Ultrasonics—Field Characterization—In Situ Exposure Estimation in Finite-Amplitude Ultrasonic Beams* (2007).
28. P. B. Rosnitskiy, P. V. Yuldashev, O. A. Sapozhnikov, A. D. Maxwell, W. Kreider, M. R. Bailey, and V. A. Khokhlova, IEEE Trans. Ultrason., Ferroelectr. Freq. Control **64** (2), 374 (2017).
29. P. B. Rosnitskiy, P. V. Yuldashev, and V. A. Khokhlova, Acoust. Phys. **61** (3), 301 (2015).
30. M. M. Karzova, M. V. Averiyanov, O. A. Sapozhnikov, and V. A. Khokhlova, Acoust. Phys. **58** (1), 81 (2012).
31. O. V. Bessonova, V. A. Khokhlova, M. R. Bailey, M. S. Canney, and L. A. Crum, Acoust. Phys. **55** (4–5), 463 (2009).
32. O. V. Rudenko and S. N. Gurbatov, Acoust. Phys. **62** (4), 418 (2016).
33. P. B. Rosnitskii, L. R. Gavrilov, P. V. Yuldashev, O. A. Sapozhnikov, and V. A. Khokhlova, Acoust. Phys. **63** (5), 531 (2017).
34. O. A. Sapozhnikov and E. A. Annenkova, Acoust. Phys. **64** (3), 299 (2018).

Translated by A. Carpenter

SPELL: 1. OK